Xu *et al. Microstructures* 2023;3:2023015
DOI: 10.20517/microstructures.2022.40

Microstructures

Research Article

Open Access

Check for updates

Novel casting CoCrNiAl eutectic high entropy alloys with high strength and good ductility

Ning Xu, Yubo Huang, Yuxian Cao, Shilei Li, Yan-dong Wang

Beijing Advanced Innovation Center for Materials Genome Engineering, State Key Laboratory for Advanced Metals and Materials, University of Science and Technology Beijing, Beijing 100083, China.

Correspondence to: Prof. Shilei Li, Beijing Advanced Innovation Center for Materials Genome Engineering, State Key Laboratory for Advanced Metals and Materials, University of Science and Technology Beijing, Beijing 100083, China. E-mail: lishilei@ustb.edu.cn; Prof. Yan-dong Wang, Beijing Advanced Innovation Center for Materials Genome Engineering, State Key Laboratory for Advanced Metals and Materials, University of Science and Technology Beijing, Beijing 100083, China. E-mail: ydwang@ustb.edu.cn

How to cite this article: Xu N, Huang Y, Cao Y, Li S, Wang Yd. Novel casting CoCrNiAl eutectic high entropy alloys with high strength and good ductility. *Microstructures* 2023;3:2023015. https://dx.doi.org/10.20517/microstructures.2022.40

Received: 2 Nov 2022 **First Decision:** 7 Dec 2022 **Revised:** 10 Feb 2023 **Accepted:** 14 Feb 2023 **Published:** 27 Feb 2023

Academic Editor: Huijun Li **Copy Editor:** Fangling Lan **Production Editor:** Fangling Lan

Abstract

Eutectic high-entropy alloys (EHEAs) have drawn increasing interest due to their fine castability as well as appealing properties in recent years. In this work, two bulk-casting $Co_{20-x/3}Cr_{20-x/3}Ni_{50-x/3}Al_{10+x}$ (x = 8 and 9) EHEAs with regular $L1_2$/B2 lamellar morphologies were successfully fabricated and studied. Both EHEAs show high ultimate strength of ~1200 MPa combined with good uniform ductility (> 9%). Post-deformation transmission electron microscopy results indicated a high density of dislocations and stacking faults in the $L1_2$ lamellae, while no obvious dislocation in the B2 phases. This work can broaden the optimization of composition design in EHEAs and provide useful guidance for further development of CoCrNiAl EHEAs.

Keywords: Eutectic high-entropy alloys, lamellar morphology, stacking faults, dislocations

INTRODUCTION

High entropy alloys (HEAs), which were proposed in 2004, have drawn increasing interest due to their appealing properties relative to conventional alloys consisting of one or two principal elements[1-4]. Despite alloying various principal elements, HEAs, frequently solidify into simple crystal structures, such as face-centered-cubic (FCC), body-centered-cubic (BCC) and hexagonal-close-packed (HCP) crystal structures or their ordered types (such as $L1_2$, B2 and $D0_{19}$)[5-10]. Generally, considering the as-cast mechanical properties of HEAs, FCC-structured HEAs exhibit good ductility but relatively low strength, while BCC or HCP-structured HEAs show high strength but limited ductility[11-13]. These single mechanical properties, poor castability and composition segregation can seriously deteriorate the further engineering applications of the as-cast HEAs[14,15].

Lu *et al.* first reported the concept of eutectic high entropy alloys (EHEAs) and developed a cast $AlCoCrFeNi_{2.1}$ EHEA with alternating FCC($L1_2$)/BCC(B2) lamellar morphologies and an outstanding combination of high strength and large ductility[16]. Recently, the mechanical properties of $AlCoCrFeNi_{2.1}$ EHEA were enhanced further by thermo-mechanical processing, that is, cold rolling in multi-steps to a reduction in thickness of ~90%, followed by annealing[15,17,18]. More recently, Shi *et al.* designed a directionally solidified $Al_{19}Fe_{20}Co_{20}Ni_{41}$ EHEA with ~50% uniform tensile elongation, three times that of conventional cast EHEAs and comparable strength, which provides novel guidance in developing new structured materials with large elongation and high fracture toughness[19]. Up to now, A wide range of cast EHEAs with outstanding mechanical properties and different compositions have been reported[20-26].

In the past years, Co-Cr-Ni-Al alloys have shown latent capacities to form conventional eutectic microstructures, which can be verified by Calculation of Phase Diagrams (CALPHAD) methods[27-29]. However, the microstructures for good mechanical properties and underlying deformation mechanisms of this type of EHEA still need more investigation. We initially designed $Co_{20-x/3}Cr_{20-x/3}Ni_{50-x/3}Al_{10+x}$ to investigate the Al content on the microstructures and mechanical properties of our CoCrNiAl alloys. Surprisingly, we found that a nominal composition of $Co_{20-x/3}Cr_{20-x/3}Ni_{50-x/3}Al_{10+x}$ (x = 8 and 9) (hereinafter named 18Al and 19Al, respectively.) can form eutectic microstructures with regular $L1_2$/B2 lamellar morphologies, which is similar with the lamellar structures in most studied as-cast EHEAs[12,14,27-29]. Electron probe microanalyzers, scanning and transmission electron microscopes were adopted to character the eutectic microstructures, chemical compositions and deformation mechanisms to reveal the origin of the good properties.

MATERIALS AND METHODS

CoCrNiAl alloys were prepared using arc-melting constituent elements with a purity of > 99.9 (wt.%). These two alloys were re-melted five times to improve the chemical homogeneity under a Ti-gettered argon atmosphere. The molten alloys were then drop-cast into a water-cooled copper mold with dimensions of 10 mm × 10 mm × 60 mm. Dog-bone-shaped tensile specimens with a cross-section area of 3.0 × 0.9 mm^2 and a gauge length of 10 mm were cut from the cast ingots by electrical discharge machining. Room-temperature tensile tests were conducted in a CMT4305 universal electronic tensile testing machine with a strain rate of 1×10^{-3} s^{-1}. At least three tensile experiments were repeated to improve the reproducibility. Crystal structures of these as-cast specimens were examined by X-ray diffraction (XRD) with Cu Ka radiation (Rigaku SmartLab). The 2θ scanning was performed in the range of 20°-100° at a scanning speed of 5°/min. Thermal behaviors of the as-cast HEAs were investigated by a differential scanning calorimeter (DSC) operated in an argon atmosphere at a heating/cooling rate of 10 °C /min. Nanoindentation tests were performed at least five tests for each phase using a G200 Nano Indenter system. During each indentation test, the depth was increased from 0 nm to 100 nm over a period of 20 s, and kept constant for 10 s. The tip contact did not extend beyond each phase. The microstructures were characterized by a field emission scanning electron microscope (Carl Zeiss Supra55) equipped with an electron backscatter diffraction (EBSD) detector (Oxford Instrument), electron probe microanalyzer (EPMA, SHIMADZU, 8050G) and transmission electron microscope (TEM) (FEI Tecnai G2 F20 operated at the voltage of 200 kV). The chemical characterizations of different phases were conducted using an energy dispersive spectroscopy (EDS) system attached to a transmission electron microscope (TEM). The EBSD and EPMA specimens were polished with a 2000-grit SiC paper, followed by electropolishing in an $HClO_4$:C_2H_6O = 1:9 solution with a direct voltage of 20 V at room temperature. TEM specimens were mechanically ground to about 50 μm thickness, punched to Φ3 mm circle sheets, and then thinned by twin-jet electro-polished using a mixture of 10% perchloric acid and 90% alcohol (vol.%) with a direct voltage of 30 V at a temperature of -18 °C.

RESULTS AND DISCUSSION

The XRD patterns of the as-cast 18Al and 19Al alloys, as shown in Figure 1A. Both 18Al and 19Al alloys have the FCC + BCC duplex phase microstructure. DSC curves of the 18Al and 19Al alloys are seen in Figure 1B. Both alloys show only one exothermic peak, confirming that 18Al and 19Al EHEAs are at the eutectic position, which can be attributed to their eutectic compositions. This phenomenon was also detected in other EHEAs, such as in $AlCoCrFeNi_{2.1}$[12], $Nb_{0.62}Fe_{1.98}Co_{1.22}Ni_{1.00}$[30], $CoCrFeNiTa_{0.4}$[31], and $CoCrFeNiMo_{0.8}$ alloys[32].

Figure 2A and D show the scanning electron microscope (SEM) images of as-cast 18Al and 19Al alloys, exhibiting that the as-cast 18Al and 19Al alloys both have a typical lamellar morphology of eutectic microstructure. The electron backscatter diffraction (EBSD) inverse pole figures and phase maps of as-cast 18Al and 19Al EHEAs are seen in Figure 2B and C, Figure 2E and F, respectively. Different lamellar growth directions were observed in the adjacent FCC grains of 18Al and 19Al EHEAs [Figure 2B and E], indicating that these EHEAs possess a different lamellar arrangement in the grains with different orientations. The EBSD phase maps in Figure 2C and F show that dark and light lamellae in Figure 2A and B are FCC and BCC phases, respectively. The corresponding content of FCC and BCC phases in 18Al EHEA is about 59.2 vol.% and 40.8 vol.%. Compared with the 18Al EHEA, 19Al EHEA has a higher content of the BCC phase, and the content of the BCC phase in 19Al EHEA is about 50.4 vol.%. Moreover, wider BCC lamellae in 19Al EHEA were observed in Figure 2F. In 18Al EHEA, $L1_2$ and B2 phases with nanoindentation hardness of 5.0 ± 0.6 GPa and 6.2 ± 0.7 GPa, respectively, while in 19Al EHEA, $L1_2$ and B2 phases with nanoindentation hardness of 4.6 ± 0.5 GPa and 5.7 ± 0.9 GPa, respectively. These results are consistent with the previous research that the B2 phase is harder than the $L1_2$ phase[19].

To better understand the microstructural features of as-cast 18Al and 19 Al EHEAs, we performed transmission electron microscopy (TEM) observation equipped with energy dispersive spectroscopy (EDS). Figure 3A and D exhibit the alternating lamellae microstructure of as-cast 18Al and 19Al EHEAs, respectively. According to the selected area electron diffraction patterns (SADPs) in Figure 3B and E, the dark and light lamellar in 18Al and 19Al EHEAs are $L1_2$ and B2 phases, respectively. $L1_2$ and B2 phases can be seen as ordered modes of FCC and BCC phases. EDS maps [Figure 3C and F] and SADPs reveal that the Ll_2 lamellae in 18Al and 19Al EHEAs enriched in Co and Cr while B2 phases in 18Al and 19Al EHEAs enriched in Ni and Al but depleted in Cr and Co. We noted that the B2 phases in 18Al are not well enriched in Ni and Al, mainly due to the B2 phases being eroded away during the TEM sample preparation, as seen in Figure 3A. The average widths of the BCC lamellae in 18Al and 19Al EHEAs are ~0.3 μm and ~0.5 μm, respectively. It is widely reported in Fe, Cr contained EHEAs that it is easy to precipitate in the form of spherical particles in the B2 phases owing to the Cr element showing a limited solid solubility[14,33-35]. While we failed to observe particles in the B2 lamellar of our 18Al and 19Al EHEAs, as exhibited by the STEM images of Figure 3A and D. This phenomenon may be ascribed to the removed Fe element in our EHEAs, which is similar to other EHEA[27]. In the recently-reported $Ni_{30}Co_{30}Cr_{10}Fe_{10}Al_{18}W_2$ and $Al_{19.25}Co_{18.86}Fe_{18.36}Ni_{43.53}$ EHEAs, the orientation relationship between the $L1_2$ and B2 phases is determined to be $[011]L1_2$ // $[\bar{1}11]$B2 and $(11\bar{1})L1_2$ // $(01\bar{1})$B2, meeting the classical K-S relationship[33,36]. This semi-coherent interface is usually accompanied by a great number of lattice misfit dislocations[33,36]. During the

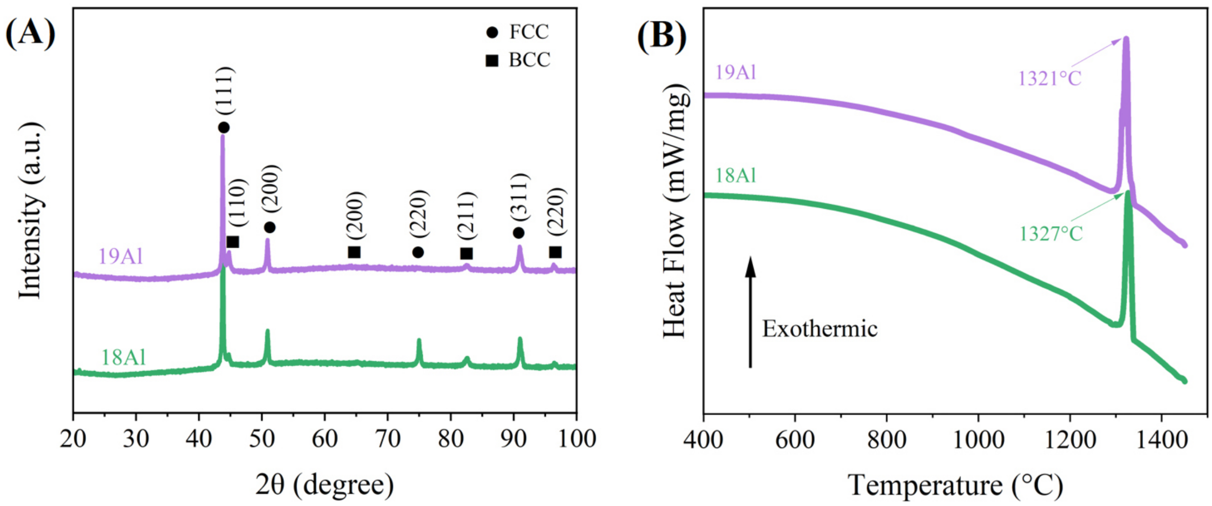

Figure 1. (A) XRD patterns of as-cast 18Al and 19Al EHEAs. (B) DSC curves of as-cast 18Al and 19Al EHEAs.

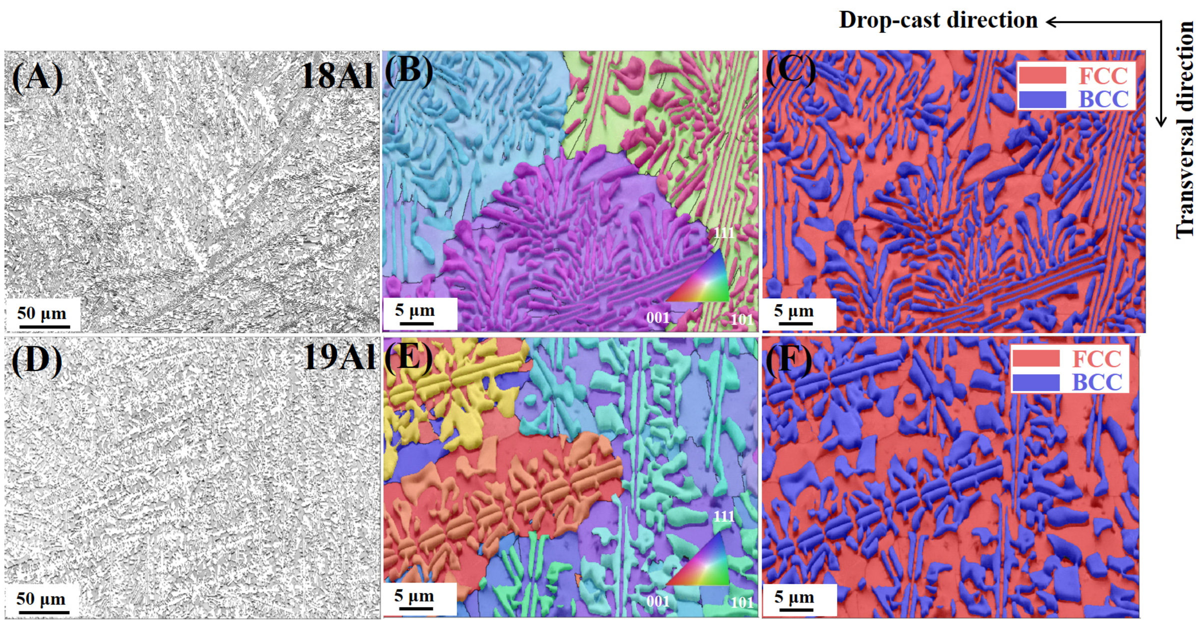

Figure 2. The microstructural features of as-cast 18Al and 19 Al EHEAs: (A-C) SEM image, inverse pole figure and phase map of 18Al EHEA; (D-F) SEM image, inverse pole figure and phase map of 19Al EHEA.

tensile deformation, this interface can block the dislocation glide further and lead to the high strength of our EHEAs.

Figure 4A displays the engineering stress-strain curves of as-cast 18Al and 19Al EHEAs tested at room temperature, exhibiting the mechanical properties including yield stress (YS), ultimate tensile strength (UTS), and total elongation (EL). The 18Al EHEA displays a yield strength of ~708 MPa, an ultimate tensile strength of ~1179 MPa, and a fracture elongation of ~0.1. The 19Al sample slightly increases the yield stress to ~734 MPa, the ultimate tensile strength to ~1219 MPa, and slightly decreases the elongation to ~0.09. 18Al and 19Al EHEAs have a high ultimate tensile strength of ~1200 MPa, which is ~ 2.3 times as strong as the as-cast $Co_{20}Cr_{20}Ni_{50}Al_{10}$ base alloy with a single-phase FCC structure. Both 18Al and 19Al EHEAs show

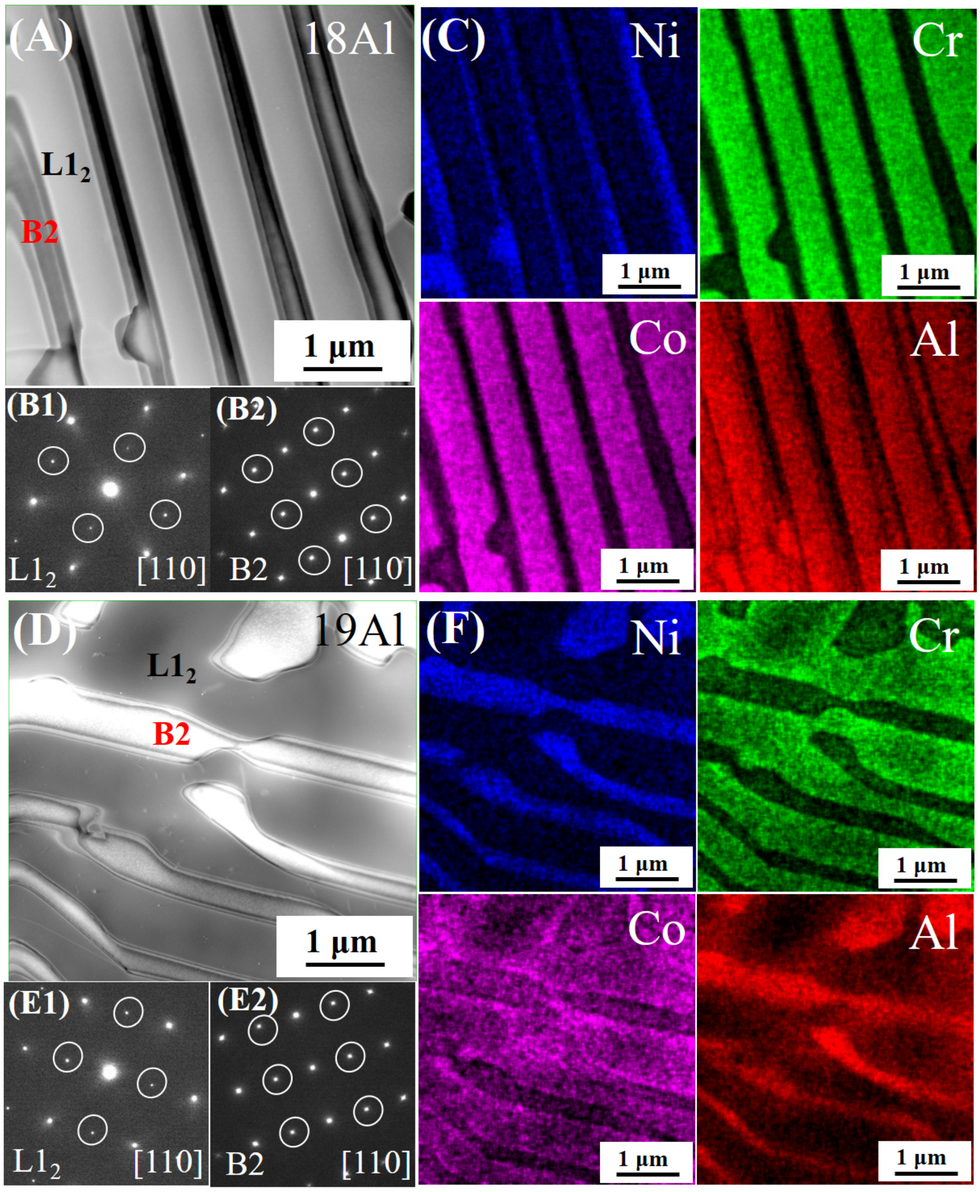

Figure 3. Scanning TEM (STEM) images showing the $L1_2$ and B2 lamellae of as-cast (A) 18Al and (D) 19Al EHEAs. Two selected-area-diffraction patterns (SADPs) of $L1_2$ and B2 lamellae in (B) 18Al and (E) 19Al EHEAs, respectively. Superlattice-diffraction spots of the $L1_2$ and B2 phases are marked by white circles. Energy-dispersive spectroscopy (EDS) maps of STEM images exhibiting the distribution of Ni, Cr, Co, Al in (C) 18Al and (F) 19Al EHEAs, respectively.

high ultimate tensile strength combined with good uniform ductility. Furthermore, little necking was detected in the stress-strain curves of two EHEAs. Figure 4B gives the strain-hardening rates of both 18Al and 19Al EHEAs. The strain-hardening rates of 18Al and 19Al EHEAs first drop quickly in region I, followed by an upturn to achieve their maximum values in region II. The strain hardening rate of 19Al EHEA is higher than that of the 18Al EHEA in this region, owing to more FCC/BCC phase boundaries that could effectively create remarkable hetero-deformation induced (HDI) hardening during the tensile deformation. The soft $L1_2$ phases will start plastic deformation first in 18Al and 19Al EHEAs, while the soft $L1_2$ phases will not be able to deform flexibly because of the deformation limit imposed by the remaining elastic B2 phases[15]. Additionally, due to the wider BCC lamellae, more geometrically necessary dislocations

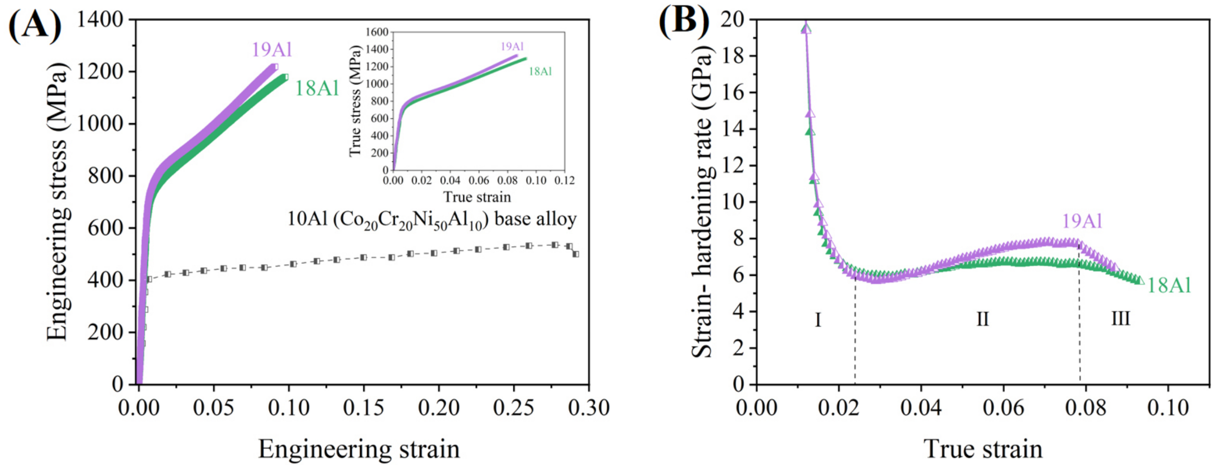

Figure 4. Mechanical responses of as-cast 18Al and 19Al EHEAs tested at room temperature. (A) The engineering stress-strain curves of 18Al and 19Al EHEAs were tested at room temperature. The inset shows the corresponding true stress-strain curve. (B) The strain hardening rate vs true strain plots of 18Al and 19Al EHEAs.

(GNDs) were prevented and piled up at FCC/BCC boundaries of 19Al in this deformation stage, resulting in larger long-range back stress in $L1_2$ phases[37-39]. The GNDs piled up at the FCC/BCC boundaries also generated forward stress in the B2 phases[37], promoting the plastic deformation of the B2 phases. When both the $L1_2$ and B2 phases were plastically deformed, the softer $L1_2$ phases would undergo larger plastic strain, leading to a heterogeneous deformation[37,38]. To accommodate the heterogeneous deformation, enough strain gradients must be present near the heterogeneous FCC/BCC surfaces, thereby producing a more remarkable HDI hardening[37] in 19Al. Finally, although the as-cast 18Al and 19Al EHEAs show an abnormal inability to sustain high strain-hardening rates over a narrow region III, they both have sufficient uniform tensile strains (> 9%).

Figure 5A and B exhibit bright-field (BF) TEM images of alternating lamellae in the ~9% strained 18Al and 19Al EHEAs. Two kinds of {111} plane traces were detected in the $L1_2$ lamellae of 18Al EHEA, as shown in Figure 5A. Figure 5B is a bright-field (BF) micrograph showing stacking faults (SFs) in the $L1_2$ lamellae of 19Al EHEA at [110] zone axis. In addition, strain-induced stacking faults were also observed in $AlCoCrFeNi_{2.1}$ EHEA[14] and additively manufactured EHEAs[40]. This scenario suggested that the stacking fault was another significant deformation type of our EHEAs besides the planar dislocation slip mentioned above in the $L1_2$ lamellae. Figure 5A and B show a high density of dislocations occurring in the $L1_2$ lamellae, while no obvious dislocations are detected in the B2 phases. In the recently-reported $AlCoCrFeNi_{2.1}$ EHEA, dislocations in the B2 lamellae can be detected in $(\bar{1}10)$ and (110) slip bands, and these dislocations could be hindered by the spherical precipitates enriched in the Cr element[14].

We investigated the fracture surfaces of 18Al and 19Al EHEAs to further reveal the damage and fracture mechanisms of the developed as-cast EHEAs at room temperature. These images of two EHEA samples in Figure 5C and D unveiled a similar fracture morphological character, namely, trench-type microstructures and several blocky phases with the cleavage character on the fracture surface[14,16,33]. More specifically, these two EHEAs both featured two types of fracture modes, i.e., brittle-type fracture in the BCC phase accompanied by a ductile fracture in the FCC phase. To better understand the blocky phases on the fracture surface of two EHEAs, we performed the EPMA analysis for the flat fracture surface of the 18Al EHEA. The EPMA images in Figure 5E reveal that the blocky phase is enriched in Ni and Al, but depleted in Co and Cr. The EPMA results indicate that blocky NiAl-rich phases are BCC precipitates. These BCC precipitates may

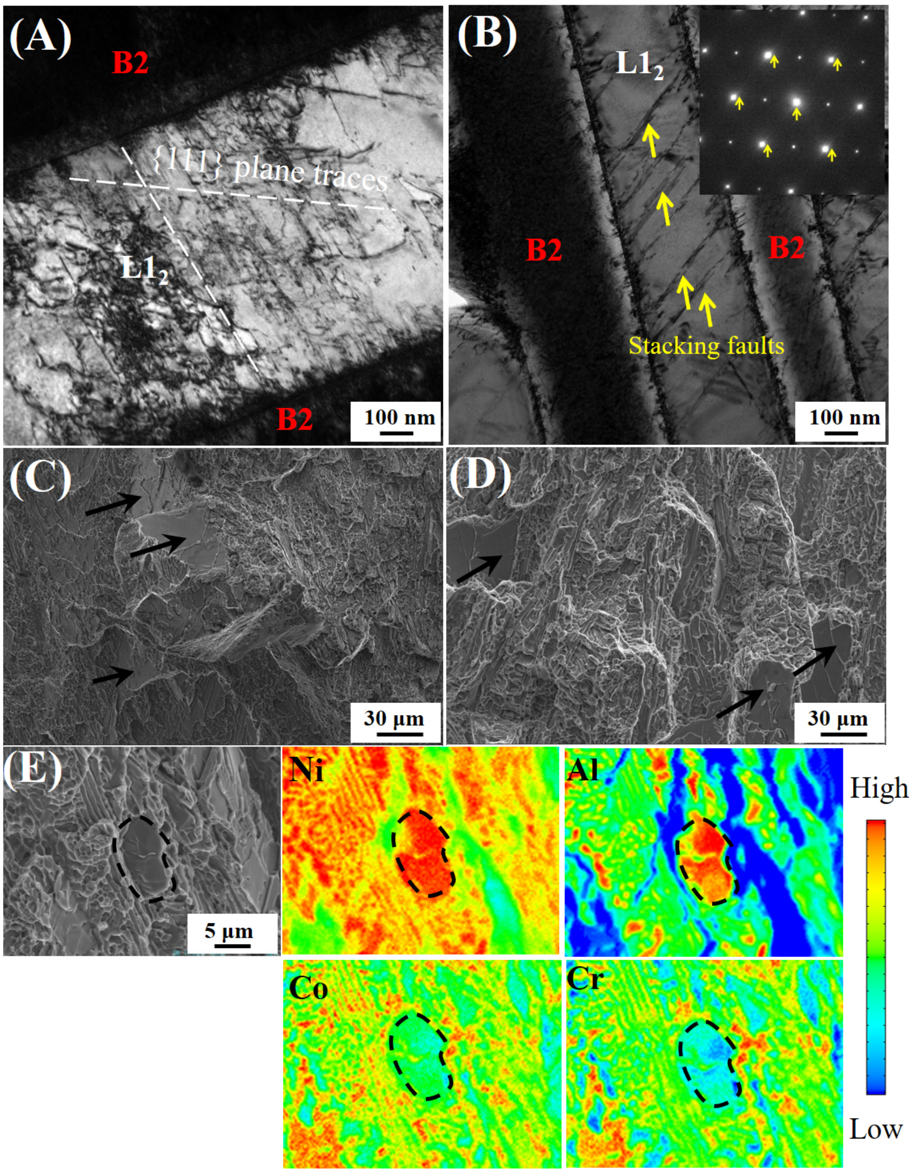

Figure 5. TEM images of alternating lamellae under the ~9% strained 18Al (A) and 19Al (B) EHEAs. The selected area electron diffraction (SAED) pattern with diffraction fringes (yellow arrows) such as trailing around diffraction spots indicates the presence of SFs. The fractography morphologies of as-cast (C) 18Al and (D) 19Al EHEAs show the mixed ductile and brittle fracture types at room temperature. Blocky phases in 18Al and 19Al EHEAs are marked by black arrows. (E) EPMA maps for the blocky phase on the fracture surface of 18Al EHEA. The blocky phase is highlighted by the black line.

be formed by a decomposition behavior, which has been detected in other EHEAs[15]. Given the blocky BCC morphology, it is reasonable to assume that the BCC particles are barely deformed while the FCC lamellae are easily stretched during the deformation. As shown in Figure 5C and D, the bright lines are stretched FCC lamellae, and the dark blocks at the bottom of the trench are BCC precipitates.

CONCLUSIONS

In summary, two novels casting CoCrNiAl EHEAs [$Co_{20-x/3}Cr_{20-x/3}Ni_{50-x/3}Al_{10+x}$ (x = 8 and 9)] composed of the $L1_2$ and B2 phases were studied. The corresponding contents of B2 phases in two EHEAs are ~40.8 vol.%

and 50.4 vol.%, respectively. The $L1_2$ lamellae in two EHEAs enriched in Co and Cr, while B2 phases in two EHEAs enriched in Ni and Al but depleted in Cr and Co. Both EHEAs have a high ultimate strength of ~1200 MPa combined with good uniform ductility (> 9%). In the ~9% strained $Co_{17.33}Cr_{17.33}Ni_{47.34}Al_{18}$ and $Co_{17}Cr_{17}Ni_{47}Al_{19}$ EHEAs, a high density of dislocations as well as stacking faults in the $L1_2$ lamellar, while no obvious dislocations are detected in the B2 phases. Moreover, Trench-type microstructures and several blocky phases with the cleavage character on the fracture surface show that brittle-type fracture in the BCC phase is accompanied by a ductile fracture in the FCC phase of two EHEAs.

DECLARATIONS

Authors' contributions

Design: Xu N

Experiments: Xu N, Huang Y, Cao Y

Data analysis: Xu N, Li S

Manuscript writing: Xu N, Li S Wang Yd

Manuscript revision and supervising: Li S, Wang Yd

Availability of data and materials

Not applicable.

Financial support and sponsorship

This work was financially supported by the National Natural Science Foundation of China (NSFC) (Nos. 52171098 and 51921001), the National High-level Personnel of Special Support Program (No. ZYZZ2021001), and the Fundamental Research Funds for the Central Universities (No. FRF-BD-20-02B).

Conflicts of interest

All authors declared that there are no conflicts of interest.

Ethical approval and consent to participate

Not applicable.

Consent for publication

Not applicable.

REFERENCES

1. Cantor B, Chang ITH, Knight P, Vincent AJB. Microstructural development in equiatomic multicomponent alloys. *Mater Sci Eng A* 2004;375-7:213-8. DOI
2. Yeh JW, Chen SK, Lin SJ, et al. Nanostructured high-entropy alloys with multiple principal elements: novel alloy design concepts and outcomes. *Adv Eng Mater* 2004;6:299-303. DOI
3. Zhang Y, Zuo TT, Tang Z, et al. Microstructures and properties of high-entropy alloys. *Prog Mater Sci* 2014;61:1-93. DOI
4. George EP, Raabe D, Ritchie RO. High-entropy alloys. *Nat Rev Mater* 2019;4:515-34. DOI
5. Lei Z, Liu X, Wu Y, et al. Enhanced strength and ductility in a high-entropy alloy via ordered oxygen complexes. *Nature* 2018;563:546-50. DOI PubMed
6. Xu N, Li S, Li R, et al. In situ investigation of the deformation behaviors of $Fe_{20}Co_{30}Cr_{25}Ni_{25}$ and $Fe_{20}Co_{30}Cr_{30}Ni_{20}$ high entropy alloys by high-energy X-ray diffraction. *Mater Sci Eng A* 2020;795:139936. DOI
7. Zhou S, Liaw PK, Xue Y, Zhang Y. Temperature-dependent mechanical behavior of an $Al_{0.5}Cr_{0.9}FeNi_{2.5}V_{0.2}$ high-entropy alloy. *Appl Phys Lett* 2021;119:121902. DOI
8. Lu W, An F, Liebscher CH. Detwinning/twin growth-induced phase transformation in a metastable compositionally complex alloy. *Microstructures* 2022;2:17. DOI

9. Zhang T, Ma S, Zhao D, et al. Simultaneous enhancement of strength and ductility in a NiCoCrFe high-entropy alloy upon dynamic tension: Micromechanism and constitutive modeling. *Int J Plast* 2020;124:226-46. DOI
10. Ma Q, Yang H, Wang Z, Shi X, Liaw PK, Qiao J. High strength and ductility in partially recrystallized $Fe_{40}Mn_{20}Cr_{20}Ni_{20}$ high-entropy alloys at cryogenic temperature. *Microstructures* 2022;2:15. DOI
11. Yan X, Liaw PK, Zhang Y. Ultrastrong and ductile BCC high-entropy alloys with low-density via dislocation regulation and nanoprecipitates. *J Mater Sci Technol* 2022;110:109-16. DOI
12. Lu Y, Dong Y, Guo S, et al. A promising new class of high-temperature alloys: eutectic high-entropy alloys. *Sci Rep* 2014;4:6200. DOI PubMed PMC
13. He J, Liu W, Wang H, et al. Effects of Al addition on structural evolution and tensile properties of the FeCoNiCrMn high-entropy alloy system. *Acta Mater* 2014;62:105-13. DOI
14. Gao X, Lu Y, Zhang B, et al. Microstructural origins of high strength and high ductility in an $AlCoCrFeNi_{2.1}$ eutectic high-entropy alloy. *Acta Mater* 2017;141:59-66. DOI
15. Shi P, Ren W, Zheng T, et al. Enhanced strength-ductility synergy in ultrafine-grained eutectic high-entropy alloys by inheriting microstructural lamellae. *Nat Commun* 2019;10:489. DOI PubMed PMC
16. Lu Y, Gao X, Jiang L, et al. Directly cast bulk eutectic and near-eutectic high entropy alloys with balanced strength and ductility in a wide temperature range. *Acta Mater* 2017;124:143-50. DOI
17. Wani I, Bhattacharjee T, Sheikh S, Bhattacharjee P, Guo S, Tsuji N. Tailoring nanostructures and mechanical properties of $AlCoCrFeNi_{2.1}$ eutectic high entropy alloy using thermo-mechanical processing. *Mater Sci Eng A* 2016;675:99-109. DOI
18. Wani IS, Bhattacharjee T, Sheikh S, et al. Ultrafine-grained $AlCoCrFeNi_{2.1}$ eutectic high-entropy alloy. *Mater Res Lett* 2016;4:174-9. DOI
19. Shi P, Li R, Li Y, et al. Hierarchical crack buffering triples ductility in eutectic herringbone high-entropy alloys. *Science* 2021;373:912-8. DOI PubMed
20. Jin X, Zhou Y, Zhang L, Du X, Li B. A novel $Fe_{20}Co_{20}Ni_{41}Al_{19}$ eutectic high entropy alloy with excellent tensile properties. *Mater Lett* 2018;216:144-6. DOI
21. Huo W, Zhou H, Fang F, Xie Z, Jiang J. Microstructure and mechanical properties of $CoCrFeNiZr_x$ eutectic high-entropy alloys. *Mater Des* 2017;134:226-33. DOI
22. Jin X, Bi J, Zhang L, et al. A new $CrFeNi_2Al$ eutectic high entropy alloy system with excellent mechanical properties. *J Alloys Compd* 2019;770:655-61. DOI
23. Wang M, Lu Y, Wang T, et al. A novel bulk eutectic high-entropy alloy with outstanding as-cast specific yield strengths at elevated temperatures. *Scr Mater* 2021;204:114132. DOI
24. Jiao W, Li T, Chang X, et al. A novel Co-free $Al_{0.75}CrFeNi$ eutectic high entropy alloy with superior mechanical properties. *J Alloys Compd* 2022;902:163814. DOI
25. Lu Y, Dong Y, Jiang H, et al. Promising properties and future trend of eutectic high entropy alloys. *Scr Mater* 2020;187:202-9. DOI
26. He F, Wang Z, Cheng P, et al. Designing eutectic high entropy alloys of $CoCrFeNiNb_x$. *J Alloys Compd* 2016;656:284-9. DOI
27. Liu F, Xiao X, Huang L, Tan L, Liu Y. Design of NiCoCrAl eutectic high entropy alloys by combining machine learning with CALPHAD method. *Mater Today Commun* 2022;30:103172. DOI
28. Wu M, Wang S, Huang H, Shu D, Sun B. CALPHAD aided eutectic high-entropy alloy design. *Mater Lett* 2020;262:127175. DOI
29. Liu Q, Liu X, Fan X, et al. Designing novel AlCoCrNi eutectic high entropy alloys. *J Alloys Compd* 2022;904:163775. DOI
30. Duan D, Wu Y, Chen H, et al. A strategy to design eutectic high-entropy alloys based on binary eutectics. *J Mater Sci Technol* 2022;103:152-6. DOI
31. Jiang H, Han K, Gao X, et al. A new strategy to design eutectic high-entropy alloys using simple mixture method. *Mater Des* 2018;142:101-5. DOI
32. Yan P, Chang J, Wang W, Zhu X, Lin M, Wei B. Eutectic growth kinetics and microscopic mechanical properties of rapidly solidified $CoCrFeNiMo_{0.8}$ high entropy alloy. *Acta Mater* 2022;237:118149. DOI
33. Shi P, Li Y, Wen Y, et al. A precipitate-free AlCoFeNi eutectic high-entropy alloy with strong strain hardening. *J Mater Sci Technol* 2021;89:88-96. DOI
34. Dong Y, Yao Z, Huang X, et al. Microstructure and mechanical properties of $AlCo_xCrFeNi_{3-x}$ eutectic high-entropy-alloy system. *J Alloys Compd* 2020;823:153886. DOI
35. Shukla S, Wang T, Cotton S, Mishra RS. Hierarchical microstructure for improved fatigue properties in a eutectic high entropy alloy. *Scr Mater* 2018;156:105-9. DOI
36. Wu Q, Wang Z, Zheng T, et al. A casting eutectic high entropy alloy with superior strength-ductility combination. *Mate Lett* 2019;253:268-71. DOI
37. Zhu Y, Wu X. Perspective on hetero-deformation induced (HDI) hardening and back stress. *Mater Res Lett* 2019;7:393-8. DOI
38. Huang C, Wang Y, Ma X, et al. Interface affected zone for optimal strength and ductility in heterogeneous laminate. *Mater Today* 2018;21:713-9. DOI
39. Rizi M, Minouei H, Lee BJ, Toroghinejad MR, Hong SI. Effects of carbon and molybdenum on the nanostructural evolution and strength/ductility trade-off in $Fe_{40}Mn_{40}Co_{10}Cr_{10}$ high-entropy alloys. *J Alloys Compd* 2022;911:165108. DOI
40. Ren J, Zhang Y, Zhao D, et al. Strong yet ductile nanolamellar high-entropy alloys by additive manufacturing. *Nature* 2022;608:62-8. DOI PubMed